

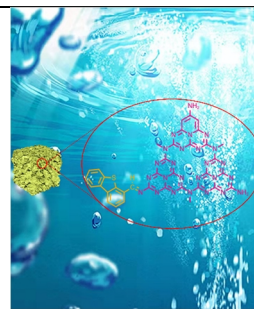
# Molecular Engineering of g-C<sub>3</sub>N<sub>4</sub> with Dibenzothiophene Groups as Electron Donor for Enhanced Photocatalytic H<sub>2</sub>-Production

Shanren Tao<sup>1</sup>, Sijie Wan<sup>1</sup>, Qinyang Huang<sup>1</sup>, Chengming Li<sup>1</sup>, Jiaguo Yu<sup>1</sup> and Shaowen Cao<sup>1\*</sup>

<sup>1</sup>State Key Laboratory of Advanced Technology for Materials Synthesis and Processing, Wuhan University of Technology, Wuhan 430070, China

**ABSTRACT** The construction of donor-acceptor (D-A) molecular structure is an attractive strategy to enhance the photocatalytic performance of polymeric semiconductors. Herein, dibenzothiophene (DBT)-4-carbaldehyde as the precursor is introduced into g-C<sub>3</sub>N<sub>4</sub> (TCN) prepared by two-step thermal polymerization to construct an intramolecular D-A type copolymer (TCN-DBT<sub>x</sub>). DFT calculation and experimental results reveal that DBT plays the role of electron donor unit to modify g-C<sub>3</sub>N<sub>4</sub>. The incorporation of DBT not only adjusts the band gap to improve reduction ability, but also induces an internal electric field with extending  $\pi$ -conjugated system for effective charge transfer. As a result, TCN-DBT<sub>x</sub> exhibits much better photocatalytic performance with an optimal hydrogen production rate of 3334  $\mu\text{mol h}^{-1} \text{g}^{-1}$ , which is 2.5 times that of TCN. This work provides a protocol for preparing high-performance g-C<sub>3</sub>N<sub>4</sub>-based photocatalysts toward various applications.

**Keywords:** carbon nitride, donor-acceptor, photocatalysis, charge transfer



## 1 INTRODUCTION

The over-consumption of traditional fossil energy has slowed down the sustainable development of human society. Photocatalytic hydrogen evolution (PHE) has shown great potential in the field of solar energy utilization and transformation and is believed to be a promising solution to the world energy crisis.<sup>[1-5]</sup> High stability and efficiency are the two most important indicators of a photocatalyst. Over the past decade, graphitic carbon nitride (g-C<sub>3</sub>N<sub>4</sub>) has gradually attracted widespread attention<sup>[6-8]</sup> because of its superior properties comprising of non-toxicity, "earth-abundant" nature, suitable band gap, stable physical and chemical properties, etc.<sup>[9-12]</sup> However, the practical application of pristine g-C<sub>3</sub>N<sub>4</sub> has encountered several obstacles, e.g., low conversion efficiency of solar energy and slow mobility of photoexcited electron-hole pairs. To solve these problems, a number of strategies have been developed, including building heterojunctions with WO<sub>3</sub>,<sup>[13]</sup> CdS,<sup>[14]</sup> ZnIn<sub>2</sub>S<sub>4</sub>,<sup>[15]</sup> etc., and loading co-catalysts with sulfide,<sup>[16]</sup> selenide,<sup>[17]</sup> single metal atoms,<sup>[18,19]</sup> and so on as well as the morphology engineering to form nanosheets,<sup>[20,21]</sup> nanocages,<sup>[22]</sup> etc. Besides, element doping<sup>[23-25]</sup> and crystallinity improvement<sup>[26]</sup> are also beneficial to the enhancement of photocatalytic performance.

Apart from the above-mentioned strategies, molecular engineering is proposed more advantageous for the modification of g-C<sub>3</sub>N<sub>4</sub>, because it is convenient to distinguish the role of grafted molecular groups as electron donor (D) or acceptor (A) based on the difference of charge distribution. For instance, a series of studies<sup>[27,28]</sup> reported that acceptor blocks were introduced into the skeleton of g-C<sub>3</sub>N<sub>4</sub> to establish D-A type copolymers. Sun et al.<sup>[29]</sup> prepared benzenesulfonyl chloride incorporated g-C<sub>3</sub>N<sub>4</sub> for enhanced H<sub>2</sub> production. Besides, Fan et al.<sup>[30]</sup> selected dibromo aromatics as the electron acceptor comonomers to react with urea and constructed successfully novel intramolecular D-A copolymers with enhanced photocatalytic H<sub>2</sub> evolution. Li et al.<sup>[31]</sup> incorporated 4,4'-(benzoc 1,2,5 thiadiazole-4,7-diyl)diphenylamine

(as an electron acceptor) into the g-C<sub>3</sub>N<sub>4</sub> networks to establish donor- $\pi$ -acceptor- $\pi$ -donor polymers for a high degree of intramolecular charge transfer.

However, by introducing electron acceptor into the structural network of g-C<sub>3</sub>N<sub>4</sub>, the reduction ability of photocatalyst is weakened. This is because the reduction ability of g-C<sub>3</sub>N<sub>4</sub> depends on the energy level of its lowest unoccupied molecular orbital (LUMO). The more negative LUMO energy level indicates that g-C<sub>3</sub>N<sub>4</sub> possesses stronger reduction ability. When g-C<sub>3</sub>N<sub>4</sub> is modified with small molecules, the LUMO for electron accumulation is determined by the low energy-level units. Usually, the LUMO of the acceptor unit is lower than that of g-C<sub>3</sub>N<sub>4</sub>. Thus, when g-C<sub>3</sub>N<sub>4</sub> is modified with acceptor units, its reduction ability will be weakened. Hence, introducing electron donor units which possess higher LUMO levels into the g-C<sub>3</sub>N<sub>4</sub> frameworks where triazine rings serve as electron acceptor is a rational way to promote the photocatalytic performance while maintaining the strong reduction ability of photoinduced electrons.

Herein, dibenzothiophene (DBT)-incorporated g-C<sub>3</sub>N<sub>4</sub> compounds were successfully synthesized by heat treatment of g-C<sub>3</sub>N<sub>4</sub> and dibenzothiophene-4-formaldehyde. DBT as an electron-rich unit plays the role of electron donor and delivers electrons to the tri-s-triazine rings (as electron acceptor), to establish a g-C<sub>3</sub>N<sub>4</sub>-based intramolecular D-A copolymer (TCN-DBT<sub>x</sub>, in which x (mg) represents the quantity of dibenzothiophene-4-formaldehyde added). This D-A copolymer can be employed as a photocatalyst with much better charge migration and separation to reduce protons, as compared to pristine g-C<sub>3</sub>N<sub>4</sub>. Under visible-light irradiation, the D-A type g-C<sub>3</sub>N<sub>4</sub> shows a steady and excellent activity of hydrogen evolution, with an optimal rate of 3334  $\mu\text{mol g}^{-1} \text{h}^{-1}$ , which is 2.5 times that of pristine g-C<sub>3</sub>N<sub>4</sub>. Such performance enhancement could be owing to the reinforced optical response, the boosted transfer and separation of excited charge carriers caused by the D-A structure modification.

## 2 RESULTS AND DISCUSSION

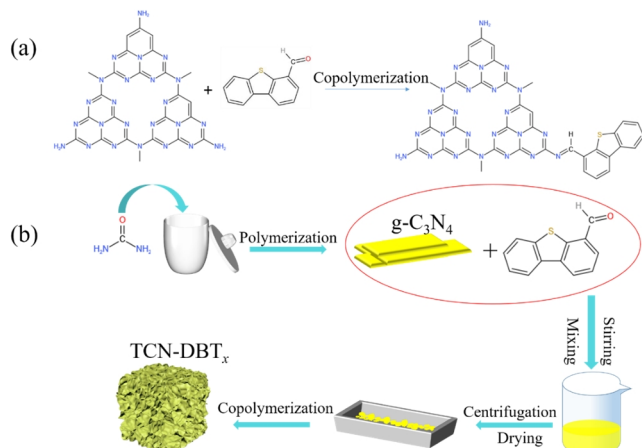


**Figure 1.** (a) Schematic illustration of formation route for TCN-DBT<sub>x</sub> and (b) experimental operation for the preparation of TCN-DBT<sub>x</sub>.

**Structure Analysis.** TCN-DBT<sub>x</sub> was fabricated by the copolymerization of a mixture of g-C<sub>3</sub>N<sub>4</sub> and DBT (Figure 1). X-ray diffraction (XRD) patterns (Figure 2a) show two typical diffraction peaks at 13.0° and 27.3° for all samples, which are assigned to (100) and (002) planes, respectively.<sup>[32,33]</sup> The former is indexed to the in-plane repeated structural packing of tri-s-triazine motifs, while the latter stems from the regular graphite-like interlayer stacking of conjugated aromatic systems.<sup>[34]</sup> The introduction of a small amount of DBT does not change the primary chemical skeleton of g-C<sub>3</sub>N<sub>4</sub>. Fourier transform infrared spectra (FTIR) of DBT-modified samples are also similar with that of TCN (Figure 2b). The sharp signal at 810 cm<sup>-1</sup> is caused by the representative breathing of heterocycles involving N in g-C<sub>3</sub>N<sub>4</sub>.<sup>[19]</sup> The peaks ranging from 1200 to 1600 cm<sup>-1</sup> are the characteristics of stretching vibration modes of tri-s-triazine (C<sub>6</sub>N<sub>7</sub>) rings.<sup>[35]</sup> The extensive absorption band emerging at the scope of 3000–3400 cm<sup>-1</sup> is related to the vibrations of N–H bonds owing to uncondensed amino groups or O–H bonds resulting from adsorbed H<sub>2</sub>O.<sup>[36]</sup> When the DBT content is increased to 16 mg, a characteristic peak corresponding to the aromatic C=C<sup>[30]</sup> appears at 1508 cm<sup>-1</sup> (Figure S1), which is also the evidence of successful incorporation of DBT into g-C<sub>3</sub>N<sub>4</sub> networks.

To acquire more detailed information about the influence of DBT on the chemical states, the XPS analyses of TCN and TCN-DBT<sub>4</sub> were conducted. The constituent elements of TCN basically comprise C, N and O (Figure 2c and Table S1). Compared with TCN, TCN-DBT<sub>4</sub> contains a tiny amount of S. According to the estimated results listed in Table S1, the atomic ratio of C to N in TCN is 0.74, while TCN-DBT<sub>4</sub> has a larger value due to the incorporation of DBT. Two peaks at 284.8 and 288.1 eV are deconvoluted for the high-resolution C 1s signals of the two samples (Figure 2d). The former of TCN results from adventitious carbon on the surface while the latter corresponds to the sp<sup>2</sup> hybridized carbon (N=C=N).<sup>[37–39]</sup> Note that the peak area at 284.8 eV of TCN-DBT<sub>4</sub> (8.06%) is increased in comparison with that of TCN (7.61%) due to the presence of aromatic rings in DBT. The deconvoluted spectra of N 1s are mainly comprised of three peaks (Figure 2e). The signal at 398.5 eV is characteristic of the

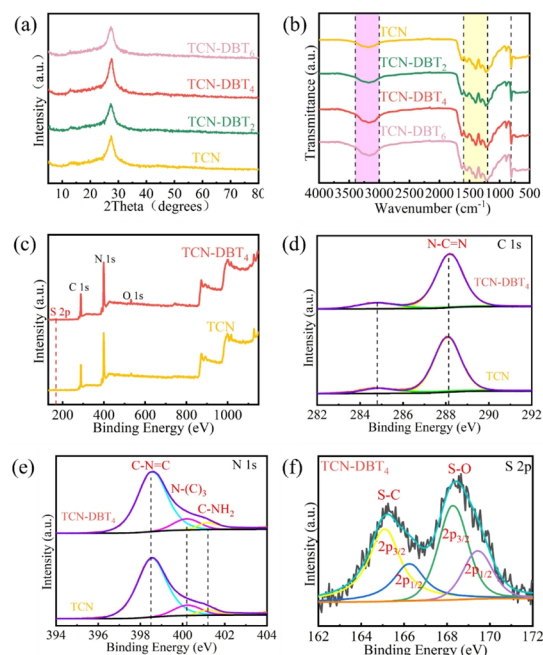


**Figure 2.** (a) XRD patterns and (b) FTIR spectra of the as-obtained samples. (c) Full survey and high-resolution X-ray photoelectron spectra (XPS) (d) C 1s, (e) N 1s of TCN and TCN-DBT<sub>4</sub>, and (f) S 2p of TCN-DBT<sub>4</sub>.

sp<sup>2</sup> hybridized aromatic N bonded to C, (C=N–C)<sup>[40]</sup> and the peak located at 400.2 eV originates from the tertiary N bonded to three carbon (N–C<sub>3</sub>).<sup>[41,42]</sup> Besides, the peak of 401.1 eV is the feature of the amino groups (–NH<sub>2</sub>).<sup>[43]</sup> Importantly, the existence of sulfur species in TCN-DBT<sub>4</sub> is readily demonstrated by the obvious signals appearing at 163.8 (S 2p<sub>3/2</sub>) and 164.9 eV (S 2p<sub>1/2</sub>) in Figure 2f, which are related to thiophene-based molecules.<sup>[36,44]</sup> Another distinct peak centered at 168.4 eV is indexed to S–O of sulfur oxides (SO<sub>x</sub>) from the partial decomposition of DBT during heat treatment in air.<sup>[45,46]</sup>

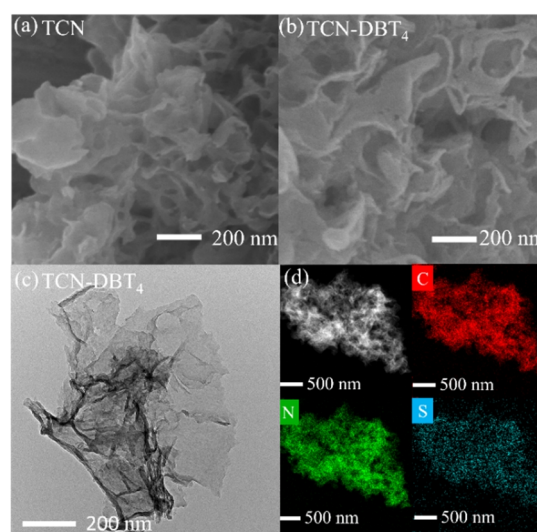


**Figure 3.** (a,b) FESEM images of TCN and TCN-DBT<sub>4</sub>. (c) TEM image and (d) corresponding elemental mapping of TCN-DBT<sub>4</sub>.

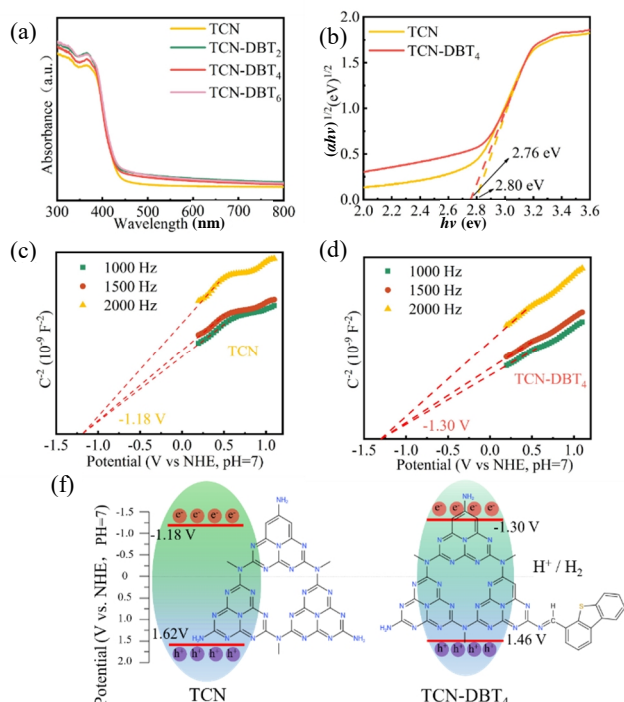


**Figure 4.** (a) UV-vis DRS and (b) plots of  $(\alpha hv)^{1/2}$  versus  $(hv)$  for TCN and TCN-DBT<sub>4</sub>. (c,d) Mott-Schottky plots collected at 1000, 1500, and 2000 Hz and (e) band alignments of TCN and TCN-DBT<sub>4</sub>.

The morphology and microstructure of various samples were investigated by field emission scanning electron microscope (FESEM) and transmission electron microscope (TEM). As depicted in Figure 3 and Figure S2, both TCN and TCN-DBT<sub>4</sub> exhibit obvious thin nanosheet structure. Note that apart from C and N, S is also uniformly distributed in the elemental mapping of TCN-DBT<sub>4</sub>. These results again prove the successful incorporation of DBT into g-C<sub>3</sub>N<sub>4</sub> frameworks without changing its main molecular structure.

The nitrogen adsorption-desorption isothermal curves and Barrett-Joyner-Halenda (BJH) pore plots are illustrated in Figure S3. Both TCN and TCN-DBT<sub>4</sub> present typical type-IV isotherms with high adsorption capacity in high relative pressure region ( $p/p_0 > 0.65$ ).<sup>[47]</sup> Such curves indicate that there are plentiful mesopores and macropores, which is consistent with the BJH pore plots. In addition, both samples possess H3-hysteresis loops, revealing the formation of slit-like pores caused by aggregation and stacking of nanosheets.<sup>[48-51]</sup> The similar structure feature also leads to the similarly high specific surface area for TCN (193 m<sup>2</sup> g<sup>-1</sup>) and TCN-DBT<sub>4</sub> (189 m<sup>2</sup> g<sup>-1</sup>), as well as similar pore volume and size (Table S2), for providing abundant reaction sites.

**Analysis of the Optical and Electronic Properties.** UV-vis diffuse reflectance spectra (DRS) were employed to explore the optical properties of TCN and TCN-DBT<sub>x</sub>. In contrast with TCN, the absorption intensity of DBT-modified samples in visible-light region was enhanced (Figure 4a). Correspondingly, the band-gaps of TCN and TCN-DBT<sub>4</sub> were determined to be 2.80 and

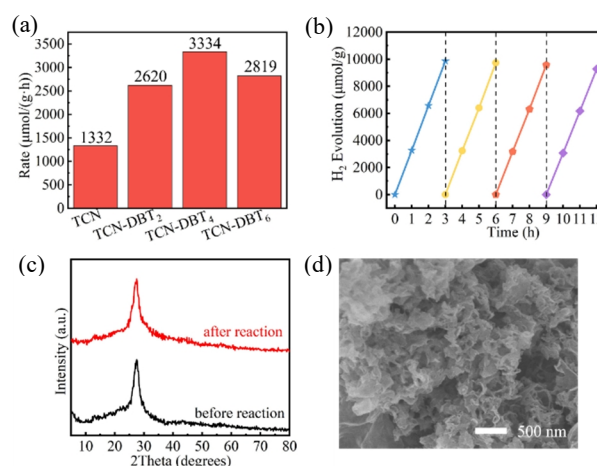


**Figure 5.** (a) PHE rates of TCN and TCN-DBT<sub>x</sub>. (b) Stability test of PHE over TCN-DBT<sub>4</sub>. (c) XRD patterns of TCN-DBT<sub>4</sub> before and after reaction. (d) FESEM image of TCN-DBT<sub>4</sub> after reaction.

2.76 eV, respectively (Figure 4b).<sup>[52,53]</sup> Mott-Schottky plots were utilized to explore the flat-band potentials ( $E_{FB}$ ) of TCN and TCN-DBT<sub>4</sub>. The curves of TCN and TCN-DBT<sub>4</sub> (Figure 4c and 4d) are characteristic of positive slope, corresponding to typical n-type semiconductor feature.<sup>[54]</sup> Generally, for n-type semiconductors, the position of the conduction band (CB) bottom is consistent with the flat band potential.<sup>[27,55]</sup> Therefore, the CB of TCN and TCN-DBT<sub>4</sub> can be roughly estimated as -1.18 and -1.30 eV, respectively. Combined with the band gap values obtained from UV-vis DRS, the band alignments are thus illustrated in Figure 4f. The result reveals that the incorporation of dibenthioophene groups could narrow the band gap of carbon nitride and cause an upshift of the CB. These alterations not only permit more electrons to participate in the reduction of protons, but also raise the reduction ability of photoinduced electrons.

**PHE Activity of As-obtained Samples.** The PHE performance of TCN and TCN-DBT<sub>x</sub> was evaluated under visible-light irradiation. As displayed in Figure 5a, TCN presents a relatively low PHE activity due to the rapid recombination of photogenerated electron-hole pairs. After the introduction of DBT into the g-C<sub>3</sub>N<sub>4</sub> frameworks, all samples show much better PHE performance than that of TCN. Particularly, TCN-DBT<sub>4</sub> shows the highest PHE rate of 3334 μmol h<sup>-1</sup> g<sup>-1</sup>, which is 2.5 times that of TCN (1332 μmol h<sup>-1</sup> g<sup>-1</sup>).

Note that after four cycles in 12 h, TCN-DBT<sub>4</sub> still remains excellent photocatalytic activity (Figure 5b). The structure and morphology of TCN-DBT<sub>4</sub> are also retained after the 4-cycle reactions, as evidenced by the XRD patterns (Figure 5c) and FESEM image (Figure 5d). These results demonstrate the superior stability of TCN-DBT<sub>4</sub> catalyst. The apparent quantum yield (AQY) of TCN and TCN-DBT<sub>4</sub> at monochromatic light irradiation of 420 nm is 0.57% and 0.82%, respectively.

**Mechanism for the Enhanced PHE Activity.** Quenching photoluminescence (PL) emission as an indicator of retarded radiation recombination implies the increased charge separation possibility.<sup>[56]</sup> PL spectra were thus measured to monitor the activity



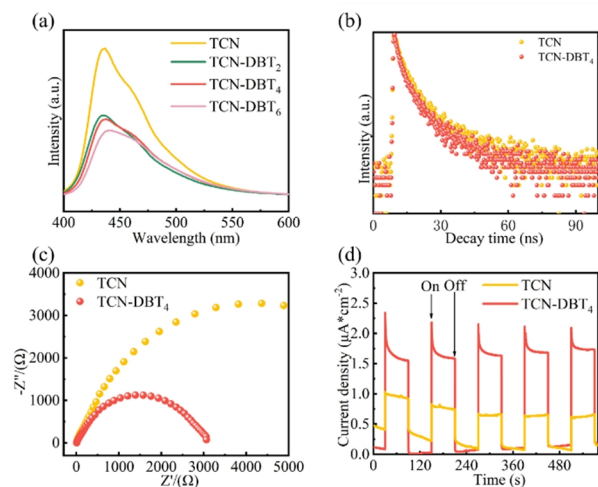


**Figure 6.** (a) PL spectra of TCN and TCN-DBT<sub>x</sub>. (b) TRPL spectra, (c) electrochemical impedance spectroscopy (EIS) plots and (d) photocurrent curves for TCN and TCN-DBT<sub>4</sub>.

of excited charge carriers within the catalysts. As shown in Figure 6a, TCN exhibits a strong PL emission at ~430 nm. After modifying g-C<sub>3</sub>N<sub>4</sub> with DBT, the peak intensity of TCN-DBT<sub>x</sub> decreases significantly with a slight red shift as the amount of DBT increases, revealing the suppression of electron-hole recombination. Time-resolved photoluminescence (TRPL) spectra were then recorded and shown in Figure 6b, where a three-exponential fitting is employed to investigate the luminescence decay curves.<sup>[19]</sup> The calculated average PL lifetime ( $\tau_{ave}$ ) of TCN and TCN-DBT<sub>4</sub> is 11.65 and 10.30 ns, respectively (Table S3). The reduced PL lifetime demonstrates the improved exciton separation.<sup>[12,57]</sup>

The EIS Nyquist plots of TCN and TCN-DBT<sub>4</sub> were also observed in dark conditions (Figure 6c). When DBT was used as electron donor to modify g-C<sub>3</sub>N<sub>4</sub>, the semicircular radius becomes significantly smaller as compared to that of TCN, revealing the greatly reduced charge transfer resistance of TCN-DBT<sub>4</sub>.<sup>[58-60]</sup> Moreover, the photocurrent intensity of TCN-DBT<sub>4</sub> is much higher than that of TCN (Figure 6d), and does not decrease noticeably within five cycles, indicating the faster dissociation efficiency of electron-hole pairs with high stability.<sup>[61-63]</sup> Further electron paramagnetic resonance (EPR) analysis (Figure 7) shows an obvious g value of ~2.0051, the typical feature of  $\pi$ -conjugated aromatic delocalization within TCN and TCN-

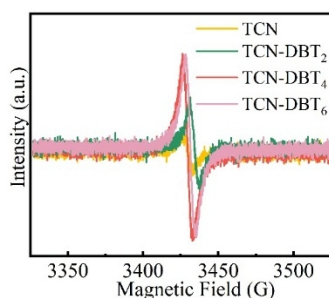


**Figure 7.** EPR spectra of TCN and TCN-DBT<sub>x</sub>.

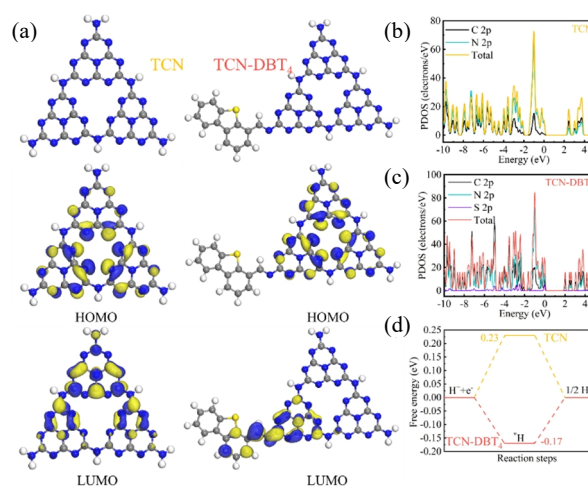


**Figure 8.** (a) Electronic structure and optimized HOMO and LUMO energy levels of TCN and TCN-DBT<sub>4</sub>. (b-c) PDOS profiles of TCN and TCN-DBT<sub>4</sub>. (d) H<sub>2</sub> adsorption free Gibbs energies

DBT<sub>x</sub>.<sup>[10,64,65]</sup> After DBT modification, the EPR signals of the sample are remarkably enhanced, revealing the existence of more unpaired electrons of the extended  $\pi$ -conjugated systems which are beneficial to the dissociation and transfer of photo-generated charge carriers.

DFT calculations were employed to investigate the electronic structures of the catalysts. Figure 8a and S4 present the spatial structure, electronic structure, optimized highest occupied molecular orbital (HOMO) and lowest unoccupied molecular orbital (LUMO) energy levels of TCN and TCN-DBT<sub>4</sub>. Compared to TCN, the HOMO change of TCN-DBT<sub>4</sub> is not obvious. But its LUMO moves from the tri-s-triazine ring to DBT and the neighboring tri-s-triazine ring. This demonstrates the incorporation of DBT contributes to the spatial separation of HOMO and LUMO, which could induce the intramolecular electron transfer under light irradiation. Besides, Figure 8b and 8c reveal the projected density of states (PDOS) of TCN and TCN-DBT<sub>4</sub>. As for TCN-DBT<sub>4</sub>, the combination of nitrogen P<sub>z</sub> orbitals generally devotes mainly to HOMO and C-N hybrid orbitals are the main contributor to LUMO, which is similar to TCN. And the TCN-DBT<sub>4</sub> effectively narrows the HOMO-LUMO gap from 2.424 eV (TCN) to 2.119 eV, consistent with the results of UV-vis DRS analysis.

As shown in Figure S5, when DBT is connected to the tri-s-triazine ring, one unit of DBT loses 0.28 e, and correspondingly, one unit of tri-s-triazine ring gains 0.28 e. This result demonstrates that DBT acts as an electron donor in the entire network of the polymer. Therefore, a built-in electric field from DBT to tri-s-triazine ring is formed, which can further promote the transfer of photogenerated electrons from HOMO to LUMO and inhibit the recombination of photogenerated electron-hole pairs. Moreover, H<sub>2</sub> adsorption free Gibbs energies ( $\Delta G_{H^+}$ ) were calculated to elucidate the kinetic mechanism of the catalytic process. In Figure 8d, the  $\Delta G_{H^+}$  value of TCN-DBT<sub>x</sub> (-0.17 eV) is significantly reduced in comparison with that of TCN (0.23 eV), indicating the easier thermodynamic process of hydrogen evolution over TCN-DBT<sub>4</sub> catalyst.<sup>[10,66]</sup>

## n CONCLUSION

In summary, intramolecular D-A modification of g-C<sub>3</sub>N<sub>4</sub> is readily achieved by the copolymerization of g-C<sub>3</sub>N<sub>4</sub> and DBT. A series of characterization and DFT calculation demonstrate that the DBT unit could act as an electron donor after incorporating into the g-C<sub>3</sub>N<sub>4</sub> frameworks. Such D-A modification of g-C<sub>3</sub>N<sub>4</sub> helps to adjust the electronic structure with more negative CB for stronger reduction ability. More importantly, the introduction of DBT into g-C<sub>3</sub>N<sub>4</sub> not only increases the electron delocalization, but also promotes the intramolecular charge transfer via inducing the internal electric field, as well as accelerating the surface catalytic process via reducing the reaction barrier. As a result, the optimal g-C<sub>3</sub>N<sub>4</sub>-based D-A copolymer shows the best hydrogen production performance (3334  $\mu\text{mol h}^{-1} \text{g}^{-1}$ ), which is 2.5 times that of pristine g-C<sub>3</sub>N<sub>4</sub>. This work introduces a facile but effective route for constructing g-C<sub>3</sub>N<sub>4</sub>-based D-A copolymer with high charge separation efficiency and excellent photocatalytic activity.

## n EXPERIMENTAL

**Synthesis of Graphitic Carbon Nitride (g-C<sub>3</sub>N<sub>4</sub>).** g-C<sub>3</sub>N<sub>4</sub> was synthesized as follows. In a typical process, 10 g of urea was placed in a crucible with a cover, then heated to 550 °C with a ramping rate of 5 °C per minute in a muffle furnace and held for 2 h. The obtained solid was cooled to room temperature and ground into fine powder for next investigation.

**Synthesis of Dibenzo thiophene-incorporated Graphitic Carbon Nitride.** The samples were prepared by thermal polymerization of a mixture of dibenzothiophene-4-formaldehyde and g-C<sub>3</sub>N<sub>4</sub>. In a typical procedure, 360 mg of g-C<sub>3</sub>N<sub>4</sub> and a certain amount of dibenzothiophene-4-formaldehyde were dispersed in a beaker containing 40 mL of deionized water and stirred vigorously for 3 hours. Then the mixture was centrifuged, and washed with deionized water and alcohol for 3 times, respectively. After that, the resulting powders were placed in an alumina porcelain boat and heated to 450 °C for 2 h in a muffle furnace at a heating rate of 5 °C per minute. The as-obtained samples were recorded as TCN-DBT<sub>x</sub> ( $x = 2, 4, 6$ ), in which  $x$  (mg) represents the quantity of dibenzothiophene-4-formaldehyde added. The sample used for comparison was prepared by the same synthetic procedure using g-C<sub>3</sub>N<sub>4</sub> as precursor without the addition of dibenzothiophene-4-formaldehyde, and denoted as TCN.

**Photocatalytic Hydrogen Evolution Tests.** At room temperature, a 100 mL three-necked flask was used as the photocatalytic hydrogen production reactor to conduct the activity test of the catalyst. 20 mg of photocatalyst was placed in 72 mL of deionized water and dispersed by ultrasonic for 10 min, and then a certain amount of H<sub>2</sub>PtCl<sub>6</sub>·6H<sub>2</sub>O aqueous solution was used as the precursor to load 1 wt% Pt on the sample as a cocatalyst by photodeposition method. Then 8 mL of triethanolamine (TEOA) was added to the above solution as a hole trapping agent, and the reactor was made a closed system using rubber stoppers and tape. Before light irradiation, the mixed aqueous solution was subjected to N<sub>2</sub> for 30 minutes under magnetic stirring to remove oxygen in the closed system. Then it was illuminated under a Xe lamp (400–800 nm) and kept magnetic stirring. One

hour later, 400  $\mu\text{L}$  of gas was extracted from the reactor with a sampler and injected into a gas chromatograph (GC-14C, Shimadzu, Japan, TCD, 5 A molecular sieve column) with N<sub>2</sub> as the carrier gas.

## n ACKNOWLEDGMENTS

This work was financially supported by the National Natural Science Foundation of China (51922081, 51961135303, 51932007, and U1705251), and National Innovation and Entrepreneurship Training Program for College Students (S202110497007).

## n AUTHOR INFORMATION

Corresponding author. Email: swcao@whut.edu.cn

## n COMPETING INTERESTS

The authors declare no competing interests.

## n ADDITIONAL INFORMATION

Supplementary information is available for this paper at <http://manu30.magtech.com.cn/jghx/EN/10.14102/j.cnki.0254-5861.2022-0068>

For submission: <https://mc03.manuscriptcentral.com/cjsc>

## n REFERENCES

- (1) Zhao, W.; Chen, Z.; Yang, X. R.; Qian, X. X.; Liu, C. X.; Zhou, D. T.; Sun, T.; Zhang, M.; Wei, G. Y.; Dissanayake, P. D.; Ok, Y. S. Recent advances in photocatalytic hydrogen evolution with high-performance catalysts without precious metals. *Renew. Sust. Energ. Rev.* **2020**, 132, 110040.
- (2) Cheng, C.; He, B. W.; Fan, J. J.; Cheng, B.; Cao, S. W.; Yu, J. G. An inorganic/organic S-scheme heterojunction H<sub>2</sub>-production photocatalyst and its charge transfer mechanism. *Adv. Mater.* **2021**, 33, 2100317.
- (3) Lin, J. D.; Yan, S.; Huang, Q. D.; Fan, M. T.; Yuan, Y. Z.; Tan, T. T. Y.; Liao, D. W. TiO<sub>2</sub> promoted by two different non-noble metal cocatalysts for enhanced photocatalytic H<sub>2</sub> evolution. *Appl. Surf. Sci.* **2014**, 309, 188–193.
- (4) Xiang, X. L.; Zhu, B. C.; Cheng, B.; Yu, J. G.; Lv, H. J. Enhanced photocatalytic H<sub>2</sub>-production activity of CdS quantum dots using Sn<sup>2+</sup> as cocatalyst under visible light irradiation. *Small* **2020**, 16, 2001024.
- (5) Yang, Y.; Zhou, C. Y.; Wang, W. J.; Xiong, W. P.; Zeng, G. M.; Huang, D. L.; Zhang, C.; Song, B.; Xue, W. J.; Li, X. P.; Wang, Z. W.; He, D. H.; Luo, H. Z.; Ouyang, Z. L. Recent advances in application of transition metal phosphides for photocatalytic hydrogen production. *Chem. Eng. J.* **2021**, 405, 126547.
- (6) Maeda, K.; Wang, X. C.; Nishihara, Y.; Lu, D. L.; Antonietti, M.; Domen, K. Photocatalytic activities of graphitic carbon nitride powder for water reduction and oxidation under visible light. *J. Phys. Chem. C* **2009**, 113, 4940–4947.
- (7) Cao, S. W.; Low, J. X.; Yu, J. G.; Jaroniec, M. Polymeric photocatalysts based on graphitic carbon nitride. *Adv. Mater.* **2015**, 27, 2150–2176.
- (8) Malik, R.; Tomer, V. K. State-of-the-art review of morphological advancements in graphitic carbon nitride (g-CN) for sustainable hydrogen production. *Renew. Sust. Energ. Rev.* **2021**, 135, 110235.
- (9) Hou, Y. T.; Guan, H. H.; Yu, J. G.; Cao, S. W. Potassium/oxygen co-doped polymeric carbon nitride for enhanced photocatalytic CO<sub>2</sub> reduction. *Appl. Surf. Sci.* **2021**, 563, 150310.

- (10) Jiang, R. R.; Lu, G. H.; Liu, J. C.; Wu, D. H.; Yan, Z. H.; Wang, Y. H. Incorporation of  $\pi$ -conjugated molecules as electron donors in g-C<sub>3</sub>N<sub>4</sub> enhances photocatalytic H<sub>2</sub>-production. *Renew. Energy* **2021**, 164, 531-540.
- (11) Wang, Y. J.; Li, Y.; Cao, S. W.; Yu, J. G. Ni-P cluster modified carbon nitride toward efficient photocatalytic hydrogen production. *Chin. J. Catal.* **2019**, 40, 867-874.
- (12) Zong, X. P.; Niu, L. J.; Jiang, W. S.; Yu, Y. M.; An, L.; Qu, D.; Wang, X. Y.; Sun, Z. C. Constructing creatinine-derived moiety as donor block for carbon nitride photocatalyst with extended absorption and spatial charge separation. *Appl. Catal. B: Environ.* **2021**, 291, 120099.
- (13) Fu, J. W.; Xu, Q. L.; Low, J. X.; Jiang, C. J.; Yu, J. G. Ultrathin 2D/2D WO<sub>3</sub>/g-C<sub>3</sub>N<sub>4</sub> step-scheme H<sub>2</sub>-production photocatalyst. *Appl. Catal. B: Environ.* **2019**, 243, 556-565.
- (14) Chen, L.; Xu, Y. M.; Chen, B. In situ photochemical fabrication of CdS/g-C<sub>3</sub>N<sub>4</sub> nanocomposites with high performance for hydrogen evolution under visible light. *Appl. Catal. B: Environ.* **2019**, 256, 117848.
- (15) Lin, B.; Li, H.; An, H.; Hao, W. B.; Wei, J. J.; Dai, Y. Z.; Ma, C. S.; Yang, G. D. Preparation of 2D/2D g-C<sub>3</sub>N<sub>4</sub> nanosheet@ZnIn<sub>2</sub>S<sub>4</sub> nanoleaf heterojunctions with well-designed high-speed charge transfer nano-channels towards high efficiency photocatalytic hydrogen evolution. *Appl. Catal. B: Environ.* **2018**, 220, 542-552.
- (16) Jiang, L. S.; Wang, K.; Wu, X. Y.; Zhang, G. K.; Yin, S. Amorphous bimetallic cobalt nickel sulfide cocatalysts for significantly boosting photocatalytic hydrogen evolution performance of graphitic carbon nitride: efficient interfacial charge transfer. *ACS Appl. Mater. Interfaces* **2019**, 11, 26898-26908.
- (17) Chen, Z.; Gao, Y. T.; Chen, F.; Shi, H. F. Metallic NiSe cocatalyst decorated g-C<sub>3</sub>N<sub>4</sub> with enhanced photocatalytic activity. *Chem. Eng. J.* **2021**, 413.
- (18) Li, X. G.; Bi, W. T.; Zhang, L.; Tao, S.; Chu, W. S.; Zhang, Q.; Luo, Y.; Wu, C. Z.; Xie, Y. Single-atom Pt as co-catalyst for enhanced photocatalytic H<sub>2</sub> evolution. *Adv. Mater.* **2016**, 28, 2427-2431.
- (19) Cao, S. W.; Li, H.; Tong, T.; Chen, H. C.; Yu, A. C.; Yu, J. G.; Chen, H. M. Single-atom engineering of directional charge transfer channels and active sites for photocatalytic hydrogen evolution. *Adv. Funct. Mater.* **2018**, 28, 1802169.
- (20) Yin, J. T.; Li, Z.; Cai, Y.; Zhang, Q. F.; Chen, W. Ultrathin graphitic carbon nitride nanosheets with remarkable photocatalytic hydrogen production under visible LED irradiation. *Chem. Commun.* **2017**, 53, 9430-9433.
- (21) Cui, Y. J.; Wang, Y. X.; Wang, H.; Cao, F.; Chen, F. Y. Polycondensation of ammonium thiocyanate into novel porous g-C<sub>3</sub>N<sub>4</sub> nanosheets as photocatalysts for enhanced hydrogen evolution under visible light irradiation. *Chin. J. Catal.* **2016**, 37, 1899-1906.
- (22) Wu, M.; Gong, Y. S.; Nie, T.; Zhang, J.; Wang, R.; Wang, H. W.; He, B. B. Template-free synthesis of nanocage-like g-C<sub>3</sub>N<sub>4</sub> with high surface area and nitrogen defects for enhanced photocatalytic H<sub>2</sub> activity. *J. Mater. Chem. A* **2019**, 7, 5324-5332.
- (23) Guo, S. E.; Tang, Y. Q.; Xie, Y.; Tian, C. G.; Feng, Q. M.; Zhou, W.; Jiang, B. J. P-doped tubular g-C<sub>3</sub>N<sub>4</sub> with surface carbon defects: universal synthesis and enhanced visible-light photocatalytic hydrogen production. *Appl. Catal. B: Environ.* **2017**, 218, 664-671.
- (24) Guo, H.; Shu, Z.; Chen, D. H.; Tan, Y. G.; Zhou, J.; Meng, F. Y.; Li, T. T. One-step synthesis of S-doped g-C<sub>3</sub>N<sub>4</sub> nanosheets for improved visible-light photocatalytic hydrogen evolution. *Chem. Phys.* **2020**, 533, 110714.
- (25) Liao, Y. W.; Wang, G. H.; Wang, J.; Wang, K.; Yan, S. D.; Su, Y. R. Nitrogen vacancy induced in situ g-C<sub>3</sub>N<sub>4</sub> p-n homojunction for boosting visible light-driven hydrogen evolution. *J. Colloid Interface Sci.* **2021**, 587, 110-120.
- (26) Wang, L. Y.; Hong, Y. Z.; Liu, E. L.; Wang, Z. G.; Chen, J. H.; Yang, S.; Wang, J. B.; Lin, X.; Shi, J. Y. Rapid polymerization synthesizing high-crystalline g-C<sub>3</sub>N<sub>4</sub> towards boosting solar photocatalytic H<sub>2</sub> generation. *Int. J. Hydrogen Energy* **2020**, 45, 6425-6436.
- (27) Che, H. N.; Liu, C. B.; Che, G. B.; Liao, G. F.; Dong, H. J.; Li, C. X.; Song, N.; Li, C. M. Facile construction of porous intramolecular g-C<sub>3</sub>N<sub>4</sub>-based donor-acceptor conjugated copolymers as highly efficient photocatalysts for superior H<sub>2</sub> evolution. *Nano Energy* **2020**, 67, 104273.
- (28) Lai, J. Y.; Zhang, W. D.; Yu, Y. X. Building sp carbon-bridged g-C<sub>3</sub>N<sub>4</sub>-based electron donor- $\pi$ -acceptor unit for efficient photocatalytic water splitting. *Mol. Catal.* **2021**, 505, 111518.
- (29) Sun, D. W.; Chen, K. L.; Huang, J. H. Benzenesulfonyl chloride-incorporated g-C<sub>3</sub>N<sub>4</sub> for photocatalytic hydrogen generation by using the hydrolysate of poly(lactic acid) as sacrificial reagent. *Appl. Catal. A-Gen.* **2021**, 628, 118397.
- (30) Fan, X. Q.; Zhang, L. X.; Cheng, R. L.; Wang, M.; Li, M. L.; Zhou, Y. J.; Shi, J. L. Construction of graphitic C<sub>3</sub>N<sub>4</sub>-based intramolecular donor-acceptor conjugated copolymers for photocatalytic hydrogen evolution. *ACS Catal.* **2015**, 5, 5008-5015.
- (31) Li, K.; Zhang, W. D. Creating graphitic carbon nitride based donor- $\pi$ -acceptor- $\pi$ -donor structured catalysts for highly photocatalytic hydrogen evolution. *Small* **2018**, 14, 1703599.
- (32) Cao, S. W.; Jiang, J.; Zhu, B. C.; Yu, J. G. Shape-dependent photocatalytic hydrogen evolution activity over a Pt nanoparticle coupled g-C<sub>3</sub>N<sub>4</sub> photocatalyst. *Phys. Chem. Chem. Phys.* **2016**, 18, 19457-19463.
- (33) Jin, Z. L.; Li, Y. B.; Hao, X. Q. Ni, Co-based selenide anchored g-C<sub>3</sub>N<sub>4</sub> for boosting photocatalytic hydrogen evolution. *Acta Phys.-Chim. Sin.* **2021**, 37, 1912033.
- (34) Wang, J.; Zhao, H.; Zhu, B. C.; Larter, S.; Cao, S. W.; Yu, J. G.; Kibria, M. G.; Hu, J. G. Solar-driven glucose isomerization into fructose via transient Lewis acid-base active sites. *ACS Catal.* **2021**, 11, 12170-12178.
- (35) Xia, P. F.; Cao, S. W.; Zhu, B. C.; Liu, M. J.; Shi, M. S.; Yu, J. G.; Zhang, Y. F. Designing a 0D/2D S-scheme heterojunction over polymeric carbon nitride for visible-light photocatalytic inactivation of bacteria. *Angew. Chem. Int. Ed.* **2020**, 59, 5218-5225.
- (36) Gong, J. Y.; Xie, Z. B.; Wang, B.; Li, Z. Q.; Zhu, Y.; Xue, J. M.; Le, Z. G. Fabrication of g-C<sub>3</sub>N<sub>4</sub>-based conjugated copolymers for efficient photocatalytic reduction of U(VI). *J. Environ. Chem. Eng.* **2021**, 9, 104638.
- (37) Li, H. F.; Ding, M. N.; Luo, L. L.; Yang, G. X.; Shi, F. Y.; Huo, Y. N. Nanomesh-structured graphitic carbon nitride polymer for effective capture and photocatalytic elimination of bacteria. *ChemCatChem* **2020**, 12, 1334-1340.
- (38) Ye, H. N.; Wang, Z. Q.; Yu, F. T.; Zhang, S. C.; Kong, K. Y.; Gong, X. Q.; Hua, J. L.; Tian, H. Fluorinated conjugated poly(benzotriazole)/g-C<sub>3</sub>N<sub>4</sub> heterojunctions for significantly enhancing photocatalytic H<sub>2</sub> evolution. *Appl. Catal. B: Environ.* **2020**, 267, 118577.
- (39) Li, H.; Li, F.; Yu, J. G.; Cao, S. W. 2D/2D FeNi-LDH/g-C<sub>3</sub>N<sub>4</sub> hybrid photocatalyst for enhanced CO<sub>2</sub> photoreduction. *Acta Phys.-Chim. Sin.* **2021**, 37, 2010073.
- (40) Kumar, A.; Prajapati, P. K.; Aathira, M. S.; Bansiwala, A.; Boukherroub, R.; Jain, S. L. Highly improved photoreduction of carbon dioxide to methanol using cobalt phthalocyanine grafted to graphitic carbon nitride as photocatalyst under visible light irradiation. *J. Colloid Interface Sci.*

2019, 543, 201-213.

- (41) Song, X. H.; Li, X.; Zhang, X. Y.; Wu, Y. F.; Ma, C. C.; Huo, P. W.; Yan, Y. S. Fabricating C and O co-doped carbon nitride with intramolecular donor-acceptor systems for efficient photoreduction of CO<sub>2</sub> to CO. *Appl. Catal. B: Environ.* **2020**, 268, 118736.
- (42) Zou, J.; Liao, G.; Jiang, J.; Xiong, Z.; Bai, S.; Wang, H.; Wu, P.; Zhang, P.; Li, X. In-situ construction of sulfur-doped g-C<sub>3</sub>N<sub>4</sub>/defective g-C<sub>3</sub>N<sub>4</sub> isotype step-scheme heterojunction for boosting photocatalytic H<sub>2</sub> evolution. *Chin. J. Struct. Chem.* **2022**, 41, 2201025-2201033.
- (43) Hayat, A.; Shaishta, N.; Mane, S. K. B.; Hayat, A.; Khan, J.; Rehman, A. U.; Li, T. H. Molecular engineering of polymeric carbon nitride based donor-acceptor conjugated copolymers for enhanced photocatalytic full water splitting. *J. Colloid Interface Sci.* **2020**, 560, 743-754.
- (44) Wang, W. R.; Li, J.; Li, Q.; Xu, Z. W.; Liu, L. N.; Chen, X. Q.; Xiao, W. J.; Yao, J. H.; Zhang, F.; Li, W. S. Side-chain-extended conjugation: a strategy for improving the photocatalytic hydrogen production performance of a linear conjugated polymer. *J. Mater. Chem. A* **2021**, 9, 8782-8791.
- (45) Zhang, Y. Z.; Shi, J. W.; Huang, Z. X.; Guan, X. J.; Zong, S. C.; Cheng, C.; Zheng, B. T.; Guo, L. J. Synchronous construction of CoS<sub>2</sub> in-situ loading and s doping for g-C<sub>3</sub>N<sub>4</sub>: enhanced photocatalytic H<sub>2</sub>-evolution activity and mechanism insight. *Chem. Eng. J.* **2020**, 401, 126135.
- (46) Xue, F.; Liu, M. C.; Cheng, C.; Deng, J. K.; Shi, J. W. Localized NiS<sub>2</sub> quantum dots on g-C<sub>3</sub>N<sub>4</sub> nanosheets for efficient photocatalytic hydrogen production from water. *ChemCatChem*. **2018**, 10, 5441-5448.
- (47) Lin, B.; An, H.; Yan, X. Q.; Zhang, T. X.; Wei, J. J.; Yang, G. D. Fish-scale structured g-C<sub>3</sub>N<sub>4</sub> nanosheet with unusual spatial electron transfer property for high-efficiency photocatalytic hydrogen evolution. *Appl. Catal. B: Environ.* **2017**, 210, 173-183.
- (48) Thommes, M.; Kaneko, K.; Neimark, A. V.; Olivier, J. P.; Rodriguez-Reinoso, F.; Rouquerol, J.; Sing, K. S. W. Physisorption of gases, with special reference to the evaluation of surface area and pore size distribution (IUPAC technical report). *Pure Appl. Chem.* **2015**, 87, 1051-1069.
- (49) Li, H.; Zhang, J.; Yu, J.; Cao, S. Ultra-thin carbon-doped Bi<sub>2</sub>WO<sub>6</sub> nanosheets for enhanced photocatalytic CO<sub>2</sub> reduction. *Trans. Tianjin Univ.* **2021**, 27, 338-347.
- (50) Li, H.; Zhu, B. C.; Cao, S. W.; Yu, J. G. Controlling defects in crystalline carbon nitride to optimize photocatalytic CO<sub>2</sub> reduction. *Chem. Commun.* **2020**, 56, 5641-5644.
- (51) Zhang, W. D.; Zhao, Z. W.; Dong, F.; Zhang, Y. X. Solvent-assisted synthesis of porous g-C<sub>3</sub>N<sub>4</sub> with efficient visible-light photocatalytic performance for NO removal. *Chin. J. Catal.* **2017**, 38, 372-378.
- (52) Zhang, Y. Z.; Huang, Z. X.; Dong, C. L.; Shi, J. W.; Cheng, C.; Guan, X. J.; Zong, S. C.; Luo, B.; Cheng, Z. N.; Wei, D. X.; Huang, Y. C.; Shen, S. H.; Guo, L. J. Synergistic effect of nitrogen vacancy on ultrathin graphitic carbon nitride porous nanosheets for highly efficient photocatalytic H<sub>2</sub> evolution. *Chem. Eng. J.* **2022**, 431.
- (53) Hu, S. W.; Shi, J. W.; Luo, B.; Ai, C. Q.; Jing, D. W. Significantly enhanced photothermal catalytic hydrogen evolution over Cu<sub>2</sub>O-rGO/TiO<sub>2</sub> composite with full spectrum solar light. *J. Colloid Interface Sci.* **2022**, 608, 2058-2065.
- (54) Lan, X. W.; Li, Q.; Zhang, Y. Z.; Li, Q.; Ricardez-Sandoval, L.; Bai, G. Y. Engineering donor-acceptor conjugated organic polymers with boron nitride to enhance photocatalytic performance towards visible-light-driven metal-free selective oxidation of sulfides. *Appl. Catal. B: Environ.* **2020**, 277, 119274.
- (55) Li, H. P.; Lee, H. Y.; Park, G. S.; Lee, B. J.; Park, J. D.; Shin, C. H.; Hou, W. G.; Yu, J. S. Conjugated polyene-functionalized graphitic carbon nitride with enhanced photocatalytic water-splitting efficiency. *Carbon* **2018**, 129, 637-645.
- (56) Zhang, Q. H.; Xia, Y.; Cao, S. W. "Environmental phosphorylation" boosting photocatalytic CO<sub>2</sub> reduction over polymeric carbon nitride grown on carbon paper at air-liquid-solid joint interfaces. *Chin. J. Catal.* **2021**, 42, 1667-1676.
- (57) Yu, H. G.; Xu, J. C.; Gao, D. D.; Fan, J. J.; Yu, J. G. Triethanolamine-mediated photodeposition formation of amorphous Ni-P alloy for improved H<sub>2</sub>-evolution activity of g-C<sub>3</sub>N<sub>4</sub>. *Sci. China Mater.* **2020**, 63, 2215-2227.
- (58) Wang, Z. L.; Chen, Y. F.; Zhang, L. Y.; Cheng, B.; Yu, J. G.; Fan, J. J. Step-scheme CdS/TiO<sub>2</sub> nanocomposite hollow microsphere with enhanced photocatalytic CO<sub>2</sub> reduction activity. *J. Mater. Sci. Technol.* **2020**, 56, 143-150.
- (59) Chen, B.; Yu, J.; Wang, R.; Zhang, X. G.; He, B. B.; Jin, J.; Wang, H. W.; Gong, Y. S. Three-dimensional ordered macroporous g-C<sub>3</sub>N<sub>4</sub>-Cu<sub>2</sub>O-TiO<sub>2</sub> heterojunction for enhanced hydrogen production. *Sci. China Mater.* **2022**, 65, 139-146.
- (60) Han, S.; Li, B.; Huang, L.; Xi, H.; Ding, Z.; Long, J. Construction of ZnIn<sub>2</sub>S<sub>4</sub>-CdIn<sub>2</sub>S<sub>4</sub> microspheres for efficient photo-catalytic reduction of CO<sub>2</sub> with visible light. *Chin. J. Struct. Chem.* **2022**, 41, 2201007-2201013.
- (61) He, F.; Meng, A. Y.; Cheng, B.; Ho, W. K.; Yu, J. G. Enhanced photocatalytic H<sub>2</sub>-production activity of WO<sub>3</sub>/TiO<sub>2</sub> step-scheme heterojunction by graphene modification. *Chin. J. Catal.* **2020**, 41, 9-20.
- (62) Yang, C.; Wang, Y. J.; Yu, J. G.; Cao, S. W. Ultrathin 2D/2D graphdiyne/Bi<sub>2</sub>WO<sub>6</sub> heterojunction for gas-phase CO<sub>2</sub> photoreduction. *ACS Appl. Energy Mater.* **2021**, 4, 8734-8738.
- (63) Chen, R.; Chen, J.; Che, H.; Zhou, G.; Ao, Y.; Liu, B. Atomically dispersed main group magnesium on cadmium sulfide as the active site for promoting photocatalytic hydrogen evolution catalysis. *Chin. J. Struct. Chem.* **2022**, 41, 2201014-2201018.
- (64) Sun, Z. Z.; Jiang, Y. B.; Zeng, L.; Huang, L. M. Intramolecular charge transfer and extended conjugate effects in donor- $\pi$ -acceptor-type mesoporous carbon nitride for photocatalytic hydrogen evolution. *ChemSusChem*. **2019**, 12, 1325-1333.
- (65) Liu, G. G.; Zhao, G. X.; Zhou, W.; Liu, Y. Y.; Pang, H.; Zhang, H. B.; Hao, D.; Meng, X. G.; Li, P.; Kako, T.; Ye, J. H. In situ bond modulation of graphitic carbon nitride to construct p-n homojunctions for enhanced photocatalytic hydrogen production. *Adv. Funct. Mater.* **2016**, 26, 6822-6829.
- (66) Che, H. N.; Li, C. M.; Li, C. X.; Liu, C. B.; Dong, H. J.; Song, X. H. Benzoyl isothiocyanate as a precursor to design of ultrathin and high-crystalline g-C<sub>3</sub>N<sub>4</sub>-based donor-acceptor conjugated copolymers for superior photocatalytic H<sub>2</sub> production. *Chem. Eng. J.* **2021**, 410, 127791.

Received: March 24, 2022

Accepted: April 8, 2022

Published: June 20, 2022